The Encore active target detector: a Multi-Sampling Ionization Chamber

B. W. Asher[a], S. Almaraz-Calderon[a], L. T. Baby[a], N. Gerken[a], E. Lopez-Saavedra[a], A. B. Morelock[a], J. F. Perello[a]

[a]*Department of Physics, Florida State University, Tallahassee, Florida 32306, USA*

Abstract

The *Encore* active target detector is a Multi Sampling Ionization Chamber developed at Florida State University (FSU). *Encore* has been successfully used to measure fusion reactions with CH_4 gas as well as (α,p) and (α,n) reactions using helium gas in the detector. The portability, self-normalizing, high-efficiency, and versatility of the *Encore* detector makes it ideal for measurements with low-intensity radioactive beams. This paper provides details on its development, operation, and analysis procedure. It also presents the results of benchmark experiments and comparison with existing data and calculations.

1. Introduction

Exotic beam facilities are at the forefront of research in experimental nuclear physics. The addition of the Facility for Rare Isotope Beams (FRIB) to the set of well-established U.S. domestic facilities like the Argonne Tandem Linac Accelerator System (ATLAS), TWINSOL facility at Notre Dame, MARS at the Texas A&M Cyclotron Institute, and RESOLUT facility at Florida State University, as well as international facilities like the Large Heavy Ion National Accelerator in France (GANIL), the Canadian national particle accelerator center (TRIUMF), and the institute of physical and chemical research in Japan (RIKEN), among others, are providing new and exciting opportunities to study nuclei away from stability that are relevant to nuclear structure, nuclear reactions, and nuclear astrophysics. However, as we push further away from stability in the chart of nuclides, beam rates become orders of magnitude lower than in the stable region. Newer detector systems are needed to address low beam currents and to perform more efficient measurements. Active target detectors are ideal to address both issues. In active target systems, the target material is also used as detection medium, measuring nuclear reactions in a large range of energies and providing large angular coverage, both of which maximize the efficiency in the detection process. For these reasons,

Email addresses: bwa15@my.fsu.edu (B. W. Asher), salmarazcalderon@fsu.edu (S. Almaraz-Calderon)

active target detectors have been developed around the world for projects that involve exotic nuclei. An example of such detectors are MUSIC [1], MAYA [2], ANASEN [3], TACTIC [4], TexAt [5], and various time projection chambers (TPCs) [6–8].

Multi Sampling Ionization Chamber (MUSIC) detectors are, in particular, an important type of active target systems. MUSIC detectors were first used for relativistic heavy ions measurements [9]. However, the MUSIC detector at Argonne National Laboratory has recently been successfully used in low energy nuclear physics research at the ATLAS facility to measure fusion reactions [10] as well as (α,p) and (α,n) reactions [11, 12].

At Florida State University (FSU), we have developed the *Encore* active target detector. *Encore* is a Multi Sampling Ionization Chamber based on the MUSIC detector at Argonne National Laboratory [1]. The primary difference between the two is in design, with *Encore* using wired field cage rather than solid aluminum plates. A difference in its operation is the use of higher voltages to optimize electron drift times, which are aimed to operate *Encore* with shorter time-of-flights and without a radio-frequency (RF) sweeper [13] used at ATLAS to increase the time between beam bunches [1, 14] in order to make a more portable detector.

Encore uses a segmented anode to measure energy losses as the beam passes through the detector. The beam and the reaction products are then identified in an event-by-event basis by their energy loss signals within the gas. Nuclear reactions that occur within the active volume of the detector are measured per strip, allowing measurements to be performed over a large range of the excitation function using a single beam energy. *Encore* was built in house at Florida State University. It has already been utilized at the John D. Fox laboratory to measure fusion, (α,n), and (α,p) reactions with stable and radioactive beams, using methane as well as helium gas in the detector. The experimental studies that can be performed with *Encore* allow investigation of stellar processes, as well as to address nuclear structure questions.

In this paper, we provide a description of the assembly, characterization, and analysis procedure of the experimental data taken with *Encore*. The performance of the detector in the measurements of the ^{16}O + ^{12}C and ^{19}F + ^{12}C fusion excitation functions above the barrier, as well as the ^{18}O(α,n)^{21}Ne and ^{18}O(α,p)^{21}F reactions, is presented along with a comparison with existing data.

2. The *Encore* detector

2.1. Assembly

Encore's housing is a 35 cm × 22 cm × 13 cm steel box with two rotatable 4.5″ ConFlat flanges on either side in order to connect to the relevant beam line. The active region of the detector is shown in Fig. 1. It consists of a cathode and an anode separated by about 11 cm. A Frisch grid sits about a centimeter away from the anode and a voltage divider makes up the field cage between the anode and the cathode.

The anode is a 32.5 cm × 12.7 cm PC board which is segmented into 18 strips. Each strip is 1.5 cm × 9 cm with a 0.7 mm gap in between. The middle 16 of which are subdivided into left and right sections with an alternating offset of 1 cm as it is shown in Fig. 2. The cathode is a solid aluminum plate the same dimensions as the anode. Between the anode and cathode is a voltage divider field cage made of Beryllium Copper wire about 0.3 mm in diameter. There are 13 layers of wire separated by about 0.75 cm. Each wire is connected by a 100 MΩ resistor starting from the cathode down to the Frisch grid. The Frisch grid is made of gold plated tungsten wires spaced 1.75 mm apart, soldered onto a PCB frame. The Frisch grid is part of the voltage divider chain and is grounded through a 6 GΩ resistor. These resistances were chosen such that the voltage drop between the cathode and the Frisch grid is only about ∼1/5 the voltage applied to the cathode. The voltage difference between the Frisch grid and the anode (ground) is the remaining 4/5 in order to amplify the signal of the drift electrons after they pass the Frisch grid. A 2200 pF capacitor is connected from the first Be-Cu wire below the cathode to ground effectively acting as a high pass filter for noise reduction. There is also a 0.1 μF capacitor connected from the Frisch grid directly to a SHV feed-thru in order to read out signals from the Frisch grid.

A negative voltage, chosen based on the gas pressure needed for the specific experiment in order to optimize the electron drift velocity for a given pressure [15], is fed to the cathode through a hermetic SHV connector. For example, in a fusion experiment using CH_4 gas, a typical voltage on the cathode is between 1 - 2 kV, depending on the pressure of the methane gas (100 - 200 torr). In experiments with helium gas, the operating voltage is typically on the order of a few hundred volts depending on the pressure of the helium (300 - 500 torr). The large difference in pressure between the gases is primarily due to the stopping power of the gas. The difference in operating voltage between the gases is due to the electron mobility within the gas as electrons drift slower within helium [16]. The gas inside the detector is held using a 2.11 mg/cm^2 thick HAVAR window at the entrance of the detector, which has been tested up to 600 torr of helium gas. A gas handling system constantly circulates the gas to ensure a constant pressure. The pressure is monitored

Figure 1: A picture of the active elements of the *Encore* detector. It consists of a cathode at the top and the segmented anode at the bottom (when mounted the detector sits upside-down to the picture's orientation). A Frisch grid is located about a centimeter away from the anode and a voltage divider makes up the field cage between the anode and the cathode.

by a precision gauge which has an error of 0.125% of it's maximum range of 500 torr [17].

In order to eliminate beam scattering off the field cage, a 3 × 3 cm hole was cut in the field cage at the height of the beam, and a frame was mounted to maintain tension on the field cage wires as shown in Fig. 1. A silicon detector or beam stop can be attached via a 4.5″ diameter ConFlat flange at the end of the detector for beam tuning.

2.2. Electronics

Encore measures energy losses in the anode as the beam passes through the detector. The number of electrons ionized by a particle is proportional to the energy deposited into the gas. These electrons then drift up along the electric field line and are collected by the anode and ultimately read by charge integration.

Each side of the detector from strip 1 to 16 of the segmented anode is read out through high-density FGG lemo cables and into 2 MPR-16 pre-amplifiers. The first and last strip (strip 0 and strip 17) are read out through BNC cables and into 2 MPR-1 pre-amplifiers. All anode pre-amplifiers are grounded at the bias input. Currently, *Encore* uses analog electronics. The MPR-16's are then fed into MSCF-16 shaper/amplifiers and then to the data acquisition system (DAQ). The MPR-1's are fed into single channel shaper/amplifiers and into a separate channel to the DAQ. The anode events are then reconstructed in an event-by-event basis during the analysis process.

The cathode and Frisch grid are also read out through MPR-1 preamplifiers. The cathode is connected to a negative bias supply that can reach voltage of ∼ -4000 V. Both the Frisch grid and the cathode can be used as a trigger since they both 'see' all the volume in the active region. However, we typically use the Frisch grid as a trigger for the DAQ since this signal is slightly faster and better shaped than that of the cathode, as well as bipolar and therefore more versatile for the electonic modules. The cathode is fed into a single channel shaper/amplifier and into an ADC. The Frisch grid signal is split after the preamplifier: one signal is fed to a fast-filter amplifier and used as a trigger, while the other is used as another ADC signal. A detailed electronics diagram of a typical *Encore* experiment is shown in Fig. 3.

At the John D. Fox laboratory, the beam can be bunched with a 12.5 MHz frequency. This is particularly important for experiments with radioactive beams where contaminants from the primary reaction are expected. We use a Time-to-Amplitude-converter (TAC) to measure the time-of-flight (ToF) of the beam. The detector trigger signal is used as the start and the radio-frequency (RF) signal from the accelerator as the stop, typically with the range set ∼ 1-5 μs. A good beam separation is obtained by plotting the ToF of the beam versus the first strip in the detector (strip 0) as shown in Fig. 4. Additional timing information can

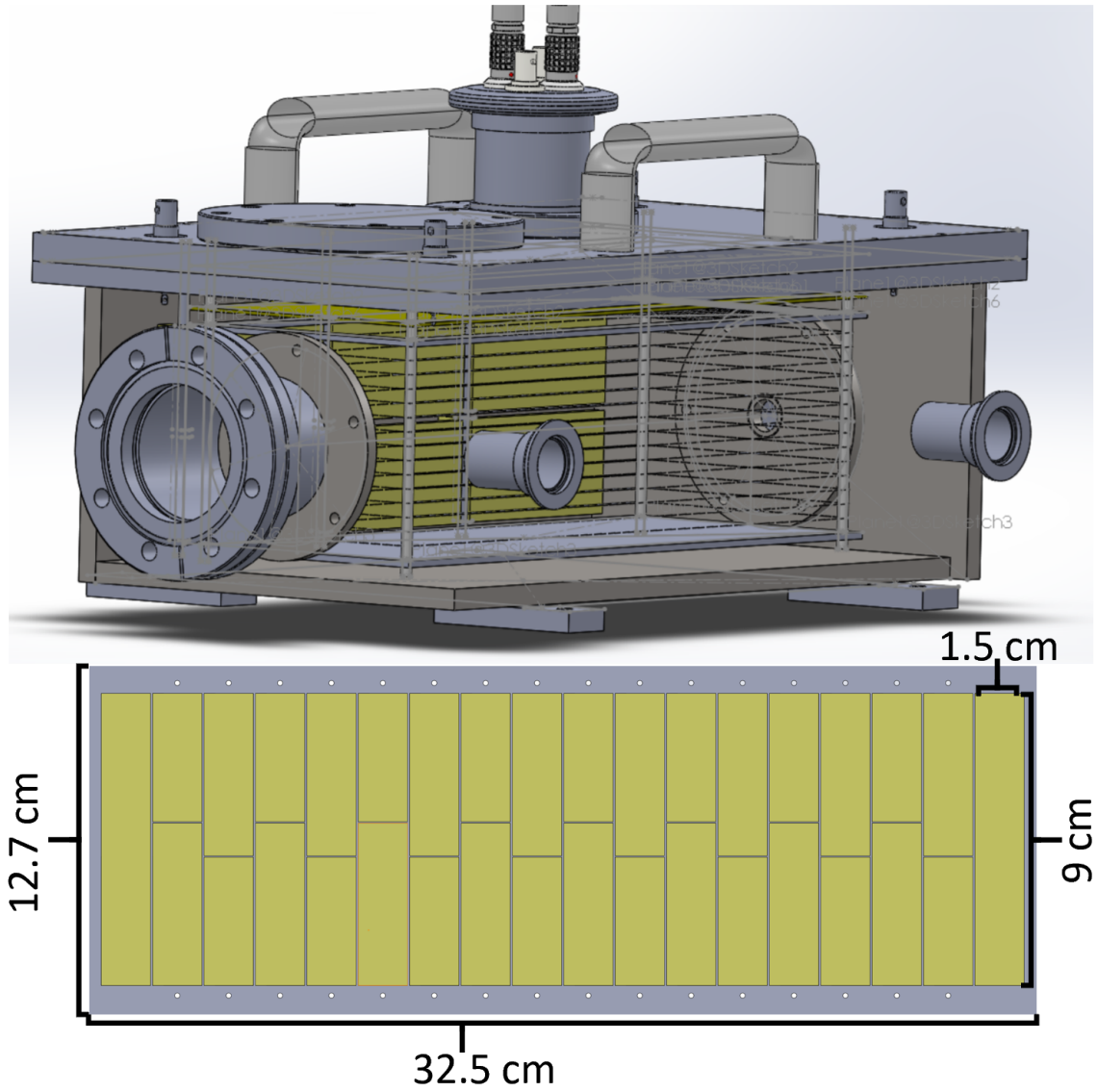

Figure 2: Upper panel: A 3D model of *Encore*. The beam passes through the center of the detector where there is a perpendicular electric field created by the field cage. This field cage is a voltage divider consisting of a cathode, wired planes, a Frisch grid, and the anode. The connections to the electronics are made through the top of the detector. The connections on the side of the detector are used for the gas handling system. Lower panel: A view of the structure of the segmented anode. It consists of 18 strips, 16 of them subdivided in left and right.

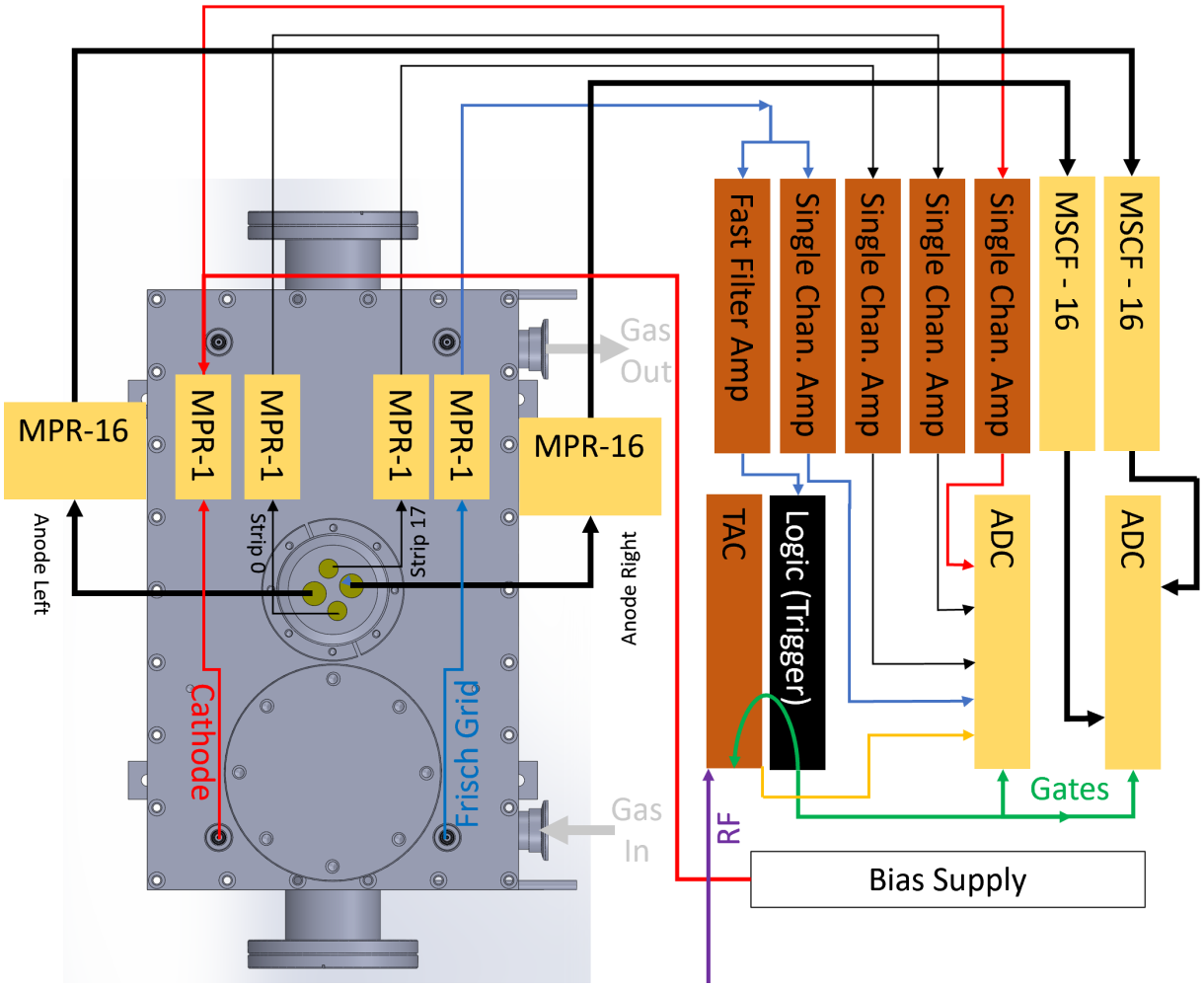

Figure 3: Electronics diagram of a typical experimental setup using *Encore* in the John D. Fox laboratory. The "Logic" box shown here is a catch-all for the various modules used including a Fan IN/Fan OUT module, Logic (and/or) module, and gate generators to make the timing and DAQ gates.

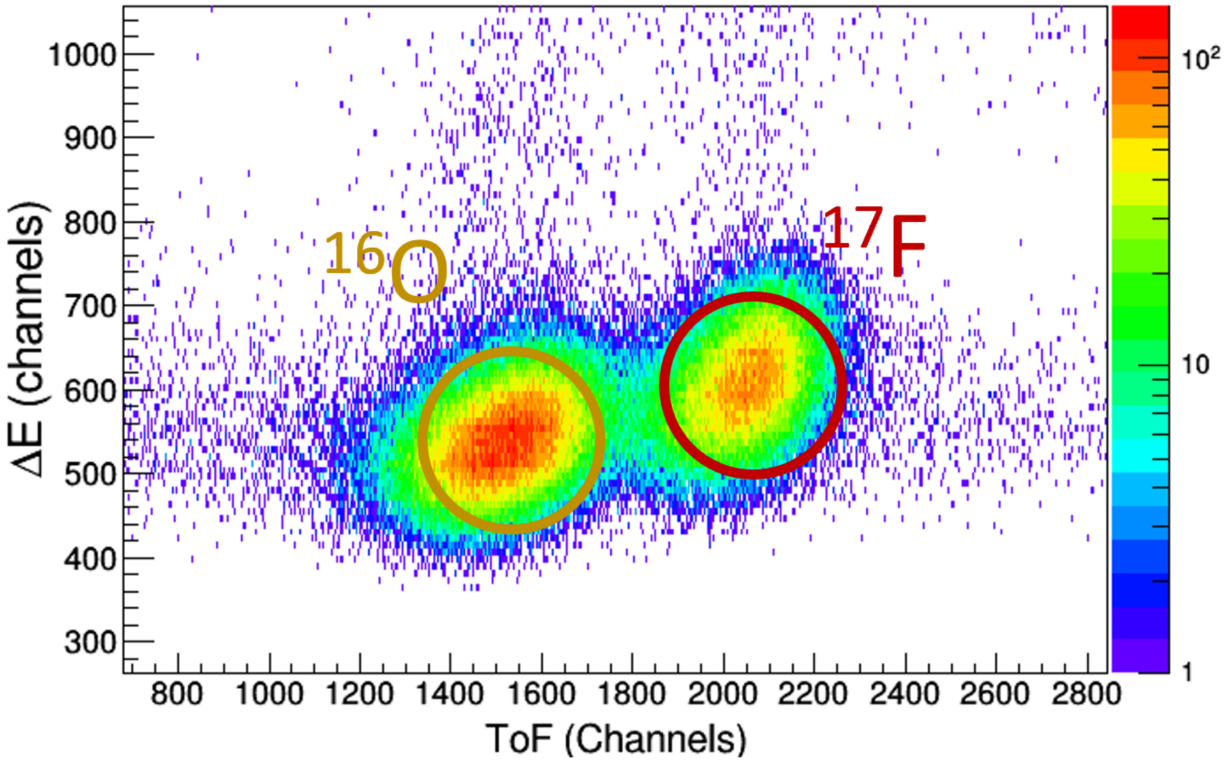

Figure 4: Time-of-flight (ToF) vs ΔE spectrum of a ^{17}F beam. The y-axis is the ΔE signal from strip 0. The x-axis is ToF of the beam. Good separation between the ^{17}F beam and its main contaminant, the primary ^{16}O beam, is observed.

be incorporated in a similar way. For the radioactive beams from the RESOLUT radioactive beam facility [18] at FSU, the timing signal from a micro-channel plate detector is sent to a second TAC.

3. *Encore*'s Operational Principles

3.1. Analysis

Encore measures energy losses as the beam passes through the detector in the different strips of the segmented anode. A beam enters into the active region, ionizing the gas and losing energy in the process. Electrons drift up towards the anode where signals are then read out through 34 channels. The anode is made up of 18 different strips, the middle 16 of which are further segmented into left and right as shown in Fig. 2. This allows for 18 distinct regions to measure the energy loss of the beam as it passes through the detector. In the analysis of the data, an event-by-event reconstruction is performed. A 'trace' is the sum of energy losses along the 18 strips of the detector (strip 0, 16 strips-right, 16 strips-left, and strip 17). *Encore*'s operation is best understood through a fusion measurement.

Strips 0 and 17 are control strips. Strip 0 provides a veto against scattering events in the entrance

window. It also defines the amount of beam that enters the detector. Strip 17 defines the amount of beam that passes through the detector without interacting.

Most of the time, the beam passes through the detector without nuclear interaction, producing a typical Bragg curve of the beam in the gas. When there is a nuclear interaction of a beam particle with a particle in the gas, a compound nucleus is formed with a higher nuclear charge (Z) than the beam. This results in a higher energy loss for that particle and therefore a larger signal read out of the anode according to the Bethe formula:

$$\frac{dE}{dx} \propto \frac{Z^2}{v^2}$$

where it can be seen that the energy loss per strip is proportional to the square of the nuclear charge of the particle (Z) and inversely proportional to the square of the velocity of the particle (v) in the medium.

The data is filtered and analyzed via 'traces' – the energy loss of a particle through the detector – shown in Fig. 5. These are sorted signals of energy loss vs. strip number, visually providing the energy loss of an event as it passes through the detector. Typically the detector only sees 'beam-like' events as shown in red in Fig. 5. Fusion events are characterized by a sudden jump in the energy loss signal. To look for signals in a given strip, beam-like events are required up until the selected strip, followed by a ΔE spike in the signal as shown by the gold traces in Fig. 5.

Guided by energy loss simulations [19], we have developed an algorithm that gain matches strips. It then it looks for a ΔE as small as one sigma away from the beam peak within a strip and sets a threshold for the following strips to ensure a clear separation between beam and fusion event. The small ΔE is set to not miss any fusion events happening in the end of a strip as it would produce a smaller ionization signal than one happening at the beginning. The algorithm then checks the height and length of the signal and ensure that the event stops within the detector since the evaporation residue will not make it to the end of the active region of the detector.

Additional filters are required to ensure the correct identification of the reaction. The segmentation of the middle 16 strips into left and right allows the inclusion of a multiplicity filter in the analysis that is used to filter out the primary source of background - scattering events. In a fusion-type event an evaporation residue is formed, leaving just one particle in the detector. In a scattering event there are two particles moving at an angle with respect to each other. The left and right segmentation allows us to see the two particles and veto that event. It is important to mention that the gains in the detector are set up so that the light particles as well as the interaction of the beam with the hydrogen in the gas are not observed.

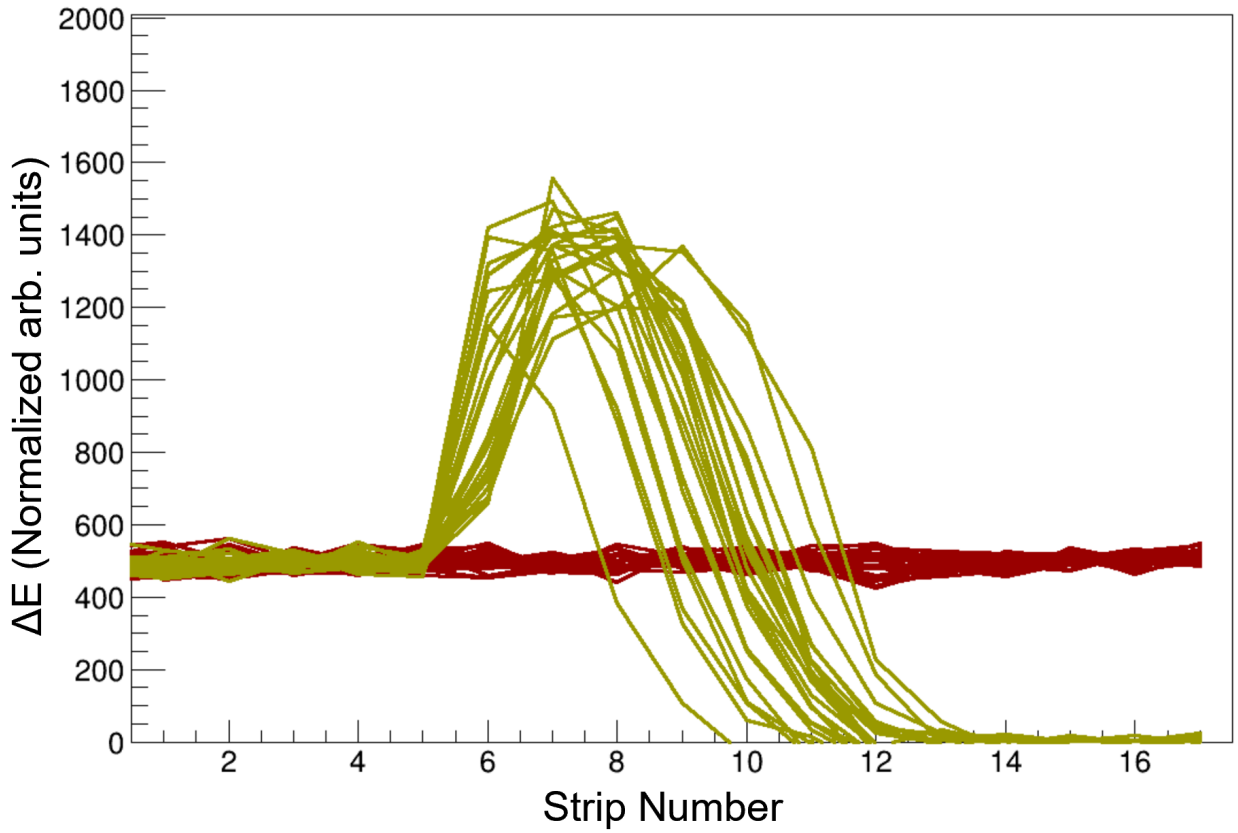

Figure 5: Energy loss traces inside of *Encore*. Typical traces of the ^{19}F beam are shown in red. The Bragg curve of the beam has been normalized to channel 500 to simplify the analysis. Typical fusion events of ^{19}F + ^{12}C happening in strip 6 are shown by the traces in gold.

An example of fusion traces occurring in strip 5 are shown in Fig. 6. In Fig. 6a, only one side of the detector fires per strip, as is shown by a characteristic zig-zag trace in the left (blue) and right (green) side of the detector. The gold trace is the sum of left + right signals. This 'multiplicity one' event is typical of a fusion reaction where the evaporation residue travels in the same direction as the beam. In Fig. 6b, the evaporation residue is emitted at a large angle with respect to the beam, and therefore, after strip 5, it is observed in only one side of the detector while the other side shows no signal.

Examples of scattering traces occurring in strip 5 are shown in Figs. 7a and 7b. In both cases, there are signals in both sides of the detector after strip 5, indicating that two particles are present. These 'multiplicity two' events are typical of scattering events.

After the correct identification of the events, the total fusion events per strip as well as beam events are counted, allowing for an absolute self-normalization of the cross sections measured.

For the case of (α,n) and (α,p) reactions, the general analysis procedure remains similar to the fusion

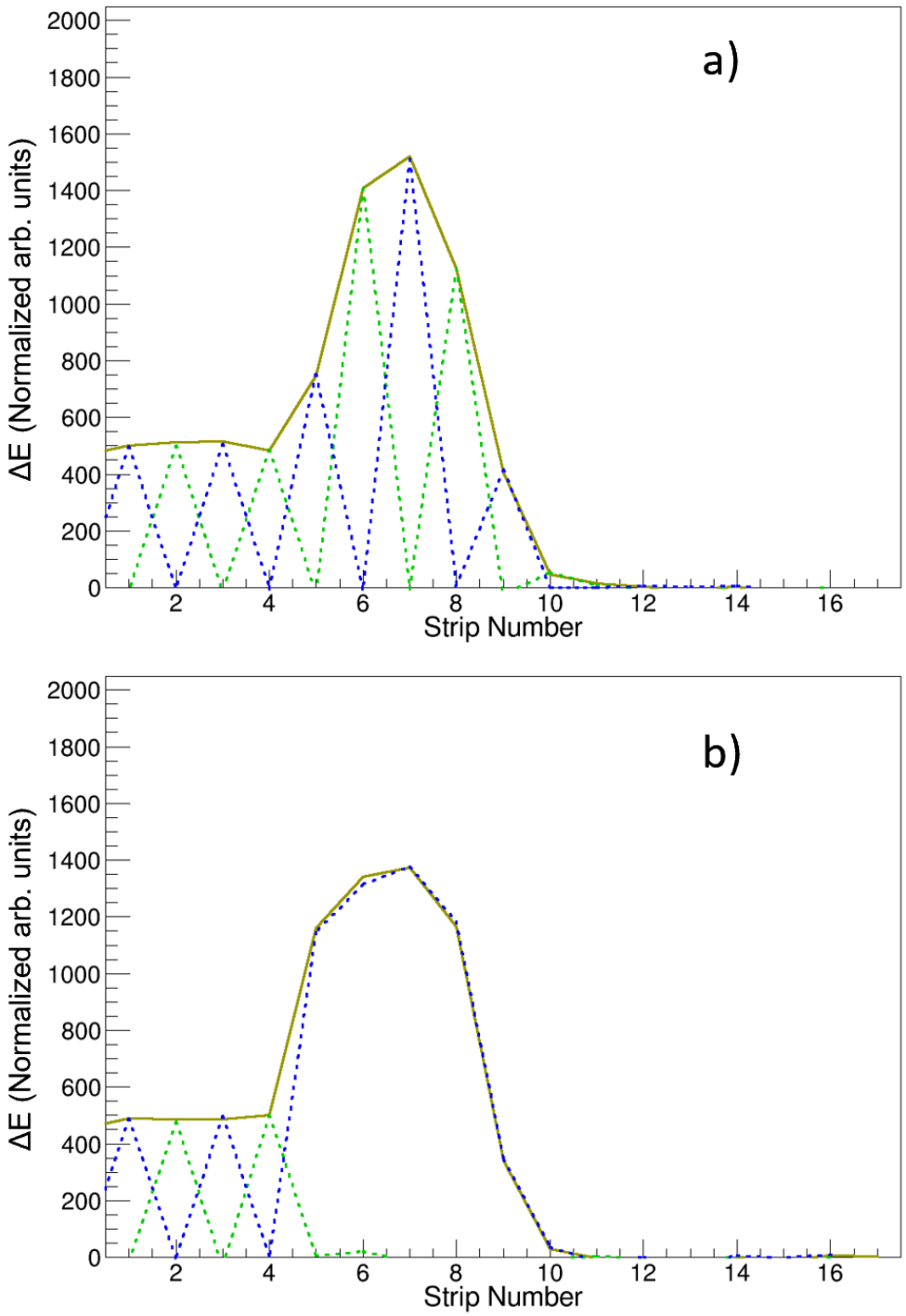

Figure 6: Typical traces in *Encore* of fusion-like events occurring in strip 5. The colors represent signals in the left (blue) and right (green) side of the segmented anode, as well as the sum of left + right signals (gold). The multiplicity information from each side of the detector is important to distinguish fusion from scattering events. In multiplicity one events, characteristic of fusion traces, only one side of the detector has a signal. Fig. 6a shows a heavy residue traveling along the beam axis (left and right alternate firing) while 6b shows a high angle heavy residue (only the left side of the detector fires as it passes through).

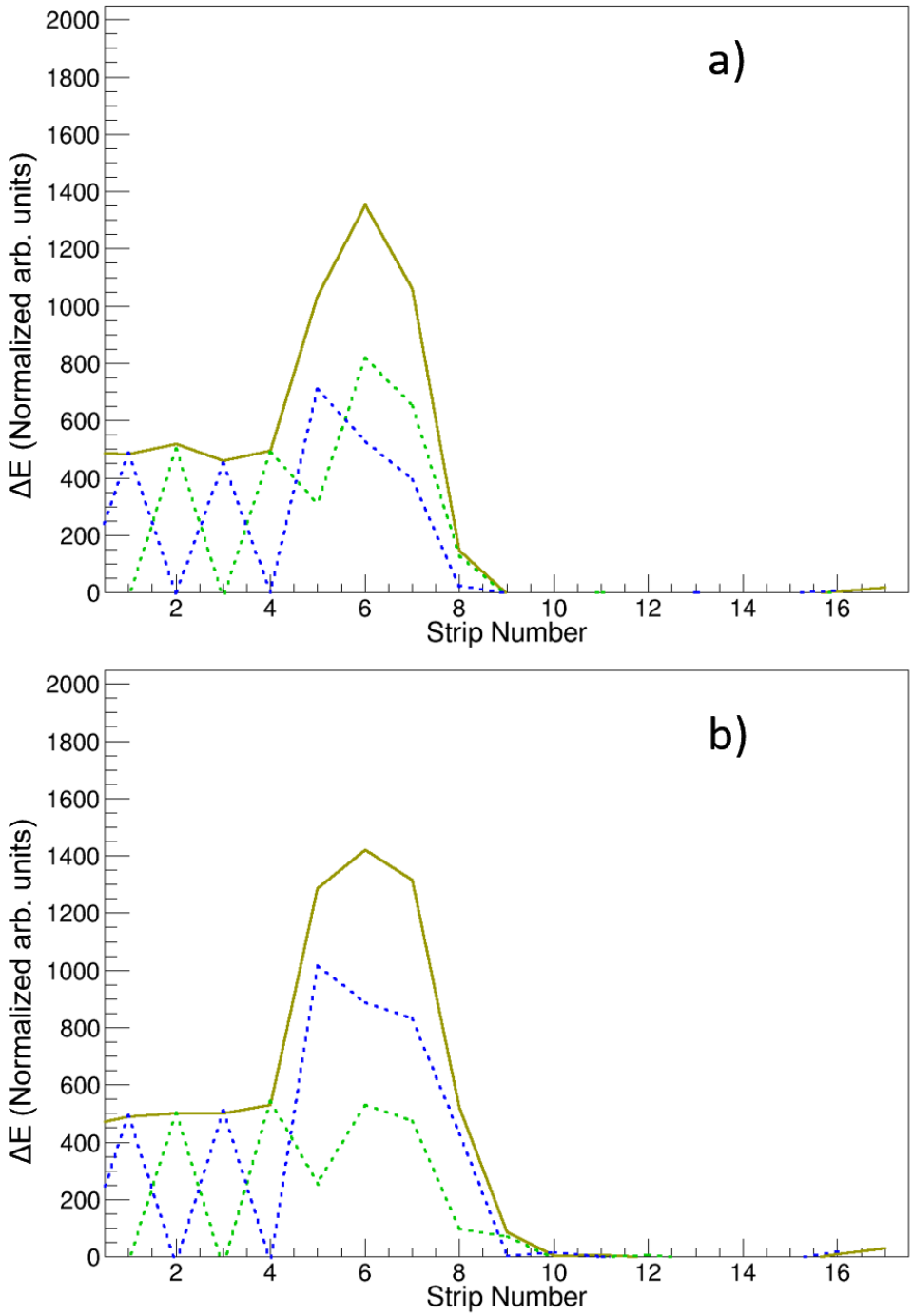

Figure 7: Typical traces in *Encore* of scattering-like events occurring in strip 5. Again, the colors represent signals in the left (blue) and right (green) side of the segmented anode, as well as the sum of left+right signals (gold). For multiplicity two events, both sides of the detector have a signal for the same strip, indicating two particles are present, which is a characteristic of scattering events. Figs. 7a and 7b both show left and right (green and blue) firing simultaneously in strips 5, 6, and 7.

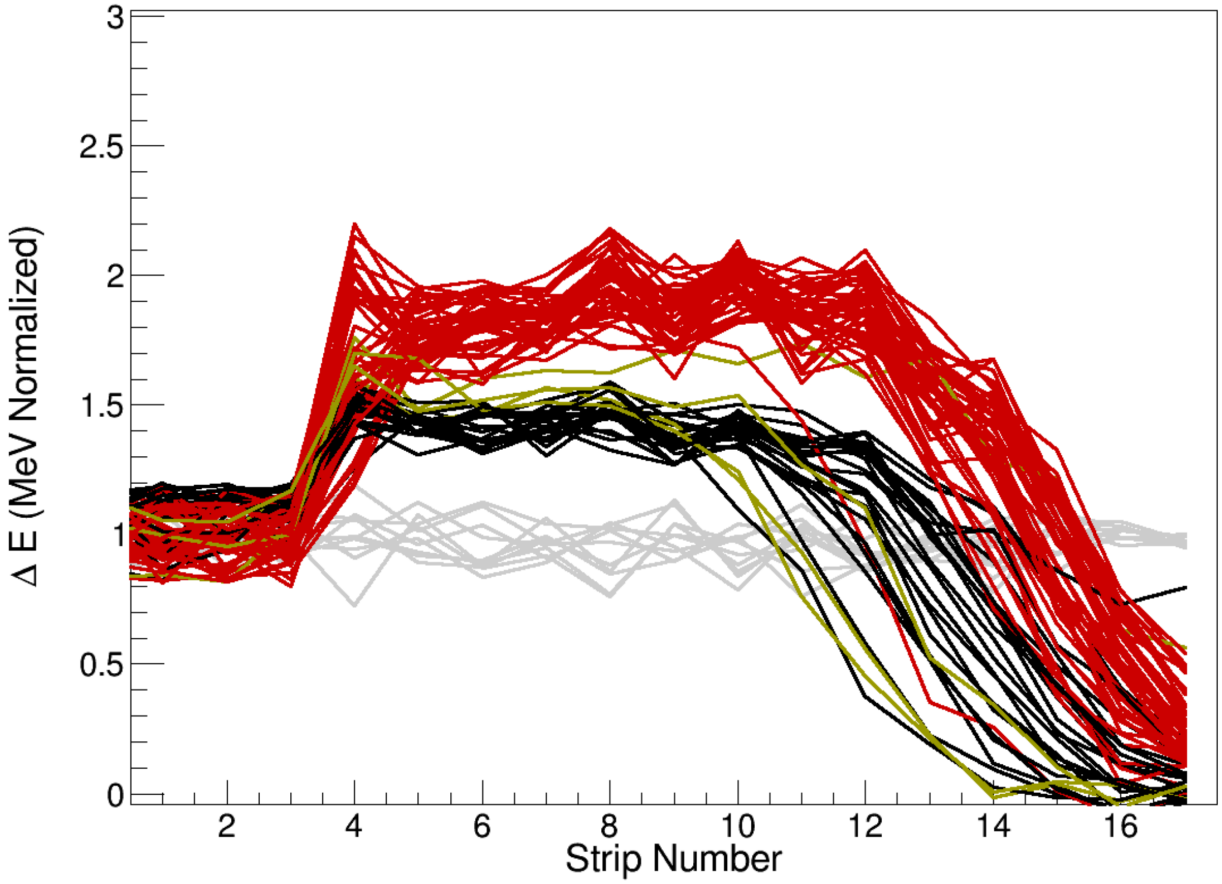

Figure 8: Traces of the ^{18}O(α,p) and ^{18}O(α,n) reactions happening in strip 4 of *Encore*. An ^{18}O beam was used to bombard *Encore*, which was filled with helium gas. Typical beam traces of ^{18}O passing through the detector are shown in grey. ^{18}O(α,α')^{18}O events are shown in black. Typical ^{18}O(α,p)^{21}F events are shown in gold and ^{18}O(α,n)^{21}Ne events are shown in red. The reactions were measured simultaneously. The expected cross section for ^{18}O(α,p)^{21}F in this region is on the order of a few mb, thus the cross section extracted for the reaction is just an upper limit.

one. For this type of experiments, *Encore* is filled with helium gas. The threshold in the ΔE signals have to be adjusted since the jump is not as drastic as it is in a fusion event. This is demonstrated by the traces of reactions of an ^{18}O beam with helium gas in *Encore* shown in Fig. 8 where ^{18}O(α,p) and ^{18}O(α,n) reactions were measured simultaneously.

Furthermore, an averaging method of the energy loss in the strips can be used to separate (α,p) and (α,n) events from beam-like events, allowing for a simultaneous measurements of both reaction channels. This procedure was first shown to work at ANL for the ^{17}O(α,n) reaction [11]. The average of several strips can be used to obtain a better separation of the different reaction channels, scattering, (α,p), and (α,n), as shown in Fig. 9.

The associated energy value for each strip is determined by the energy of the incoming beam and the gas

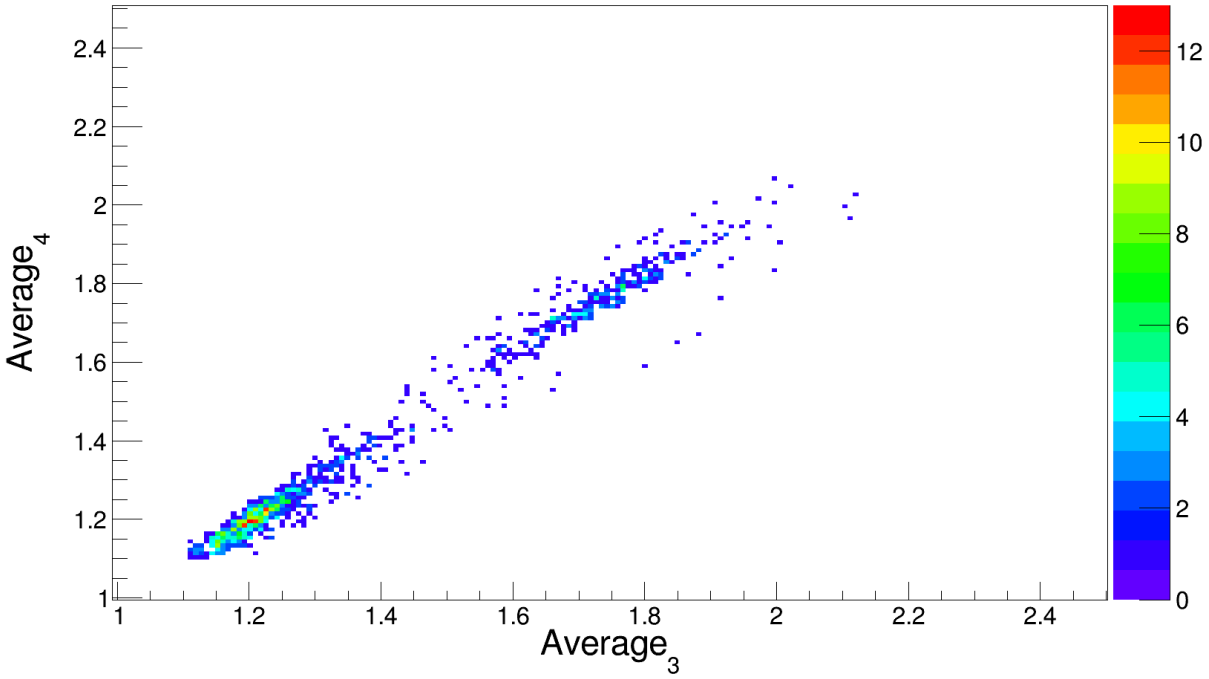

Figure 9: Average of 4-strips vs 3-strips after a reaction of ^{18}O beam with helium gas in the detector happening in strip 8. The ^{18}O(α,p)^{21}F channel is closed in this strip. The lower-left structure is the ^{18}O(α,α')^{18}O events, while the upper-right structure corresponds to ^{18}O(α,n)^{21}Ne events clearly separated from the scattering events.

pressure within the detector. LISE++ [20] is used to calculate the energy loss of the beam within a specific strip, assuming that the reaction happened at the middle of the strip, the error bars in the energy are due to the size of the strips. This procedure was validated at Argonne National Laboratory where the MUSIC detector was attached to the Split-Pole Spectrograph (SPS) so that the energy loss calculations with LISE++ could be compared with the energies measured in the focal plane detector of the SPS [1]. In the case of *Encore*, a silicon detector mounted in the back of the detector is also used to validate the energy loss calculations of the beam in the gas. This silicon detector is primarily used for beam tuning without gas in the detector. However, as gas is gradually added to *Encore*, the energy loss calculations from LISE++ are compared with the measurements in the silicon detector in order to validate the energy loss of the beam through the gas. Although at typical operating gas pressures, the beam stops before reaching the silicon detector, and the behavior of the Bragg curve of the beam and its components are also used as calibration points for the energy assignments. This is highlighted by the calibrated Bragg curve spectrum in *Encore* taken from our radioactive ^{17}F experiment shown in Fig. 10a and 10b. In this instance, the ^{17}F beam does not stop within the active region, but both the primary $^{16}O^{8+}$ and a $^{16}O^{7+}$ contaminant do. The Bragg curves from LISE++ calculations shown by the solid (^{17}F) and dashed ($^{16}O^{8+}$, and $^{16}O^{7+}$) curves are in good agreement with the measured values in *Encore*, especially well before the Bragg peak. It is important to point out that in analysis of this specific case, the $^{16}O^{7+}$ component was further gated out using the timing information as it was shown in Fig 4, and that typically only up to strip 13 is effectively used to extract a cross section since the analysis program requires additional strips to correctly identify the events in the detector.

Discrepancies between energy loss calculations have been reported for more exotic systems than the ones reported here [21, 22]. Therefore, energy loss effects have to be further studied as more exotic beams become available.

3.2. Beam Rate Characteristics

Encore is designed to be used with low intensity radioactive beams and operated at parameters optimal for the electron drift velocity. For example, with CH_4 as a counting gas, average beam intensities of up to 2.5×10^4 pps have been used while with helium gas in the detector up to 1×10^4 pps. However, measurements with more intense beams are desired. The intrinsic limit is the time that it takes the ionized electrons to drift to the anode. The two main obstacles to increasing the beam intensity are detector breakdown and pile-up signals.

As the beam rate increases, there are also more pileup events. With *Encore*, we can mark these events

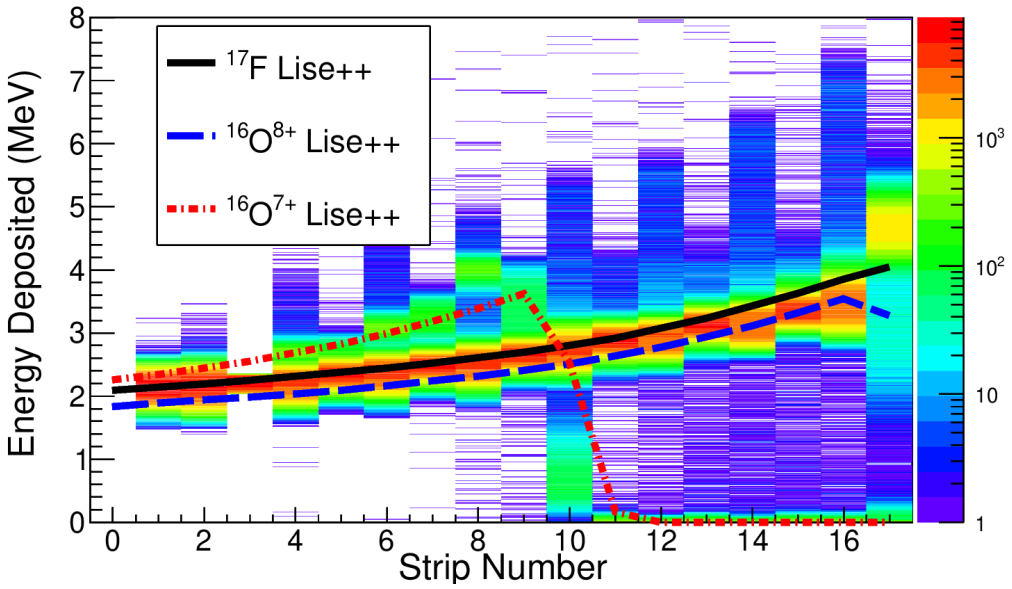

(a) Calibrated Bragg curve for the ^{17}F beam component passing through *Encore*.

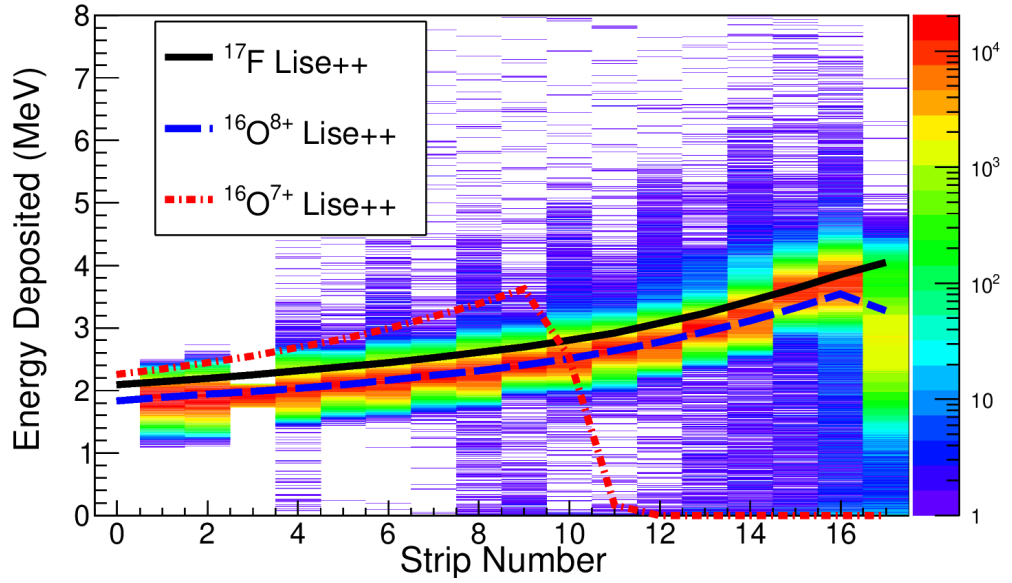

(b) Calibrated Bragg curve for the ^{16}O beam component passing through *Encore*.

Figure 10: Bragg curves measured in *Encore*. The solid black line, blue dotted lines, and the red dot-dashed lines represent ^{17}F, ^{16}O^{8+}, and ^{16}O^{7+} Bragg curves, respectively, as calculated by LISE++. The beam components in the spectra have been previously gated using its respective time of arrival to the detector shown in Fig. 4. Fig. 10a is a calibrated spectrum using the ^{17}F component of the beam while fig. 10b is a calibrated spectrum using the ^{16}O^{8+} component of the beam.

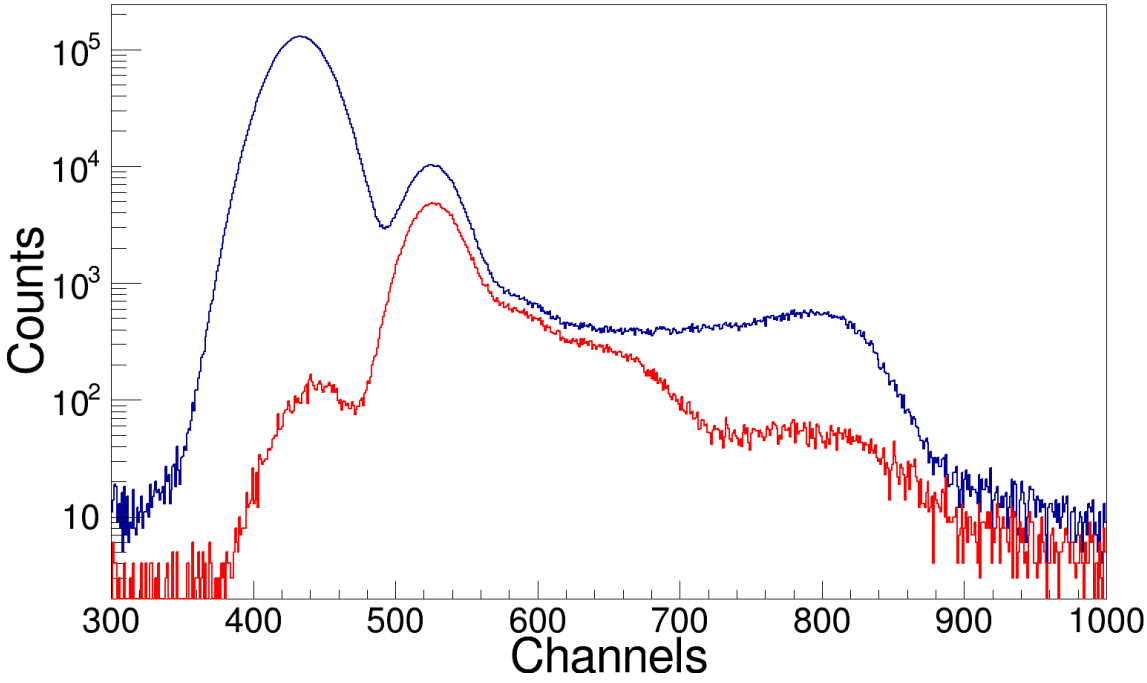

Figure 11: Pileup events within the detector as seen in Strip 2. As the incoming beam rates are increased, pileup in the detector are observed as structures in channels ~350 and above (blue). A second trigger is used to tag these pile-up events as overlapping signals from the trigger (red) and veto the DAQ, reducing the computer dead-time. See text for details.

to either throw them away in the analysis or use them as a veto on the entire DAQ to reduce the computer dead-time. The trigger signal from the Frisch grid is split to make a second copy in coincidence with a slightly delayed gate (60 ns) so that two overlapping events are flagged. We then feed the primary trigger to the start of a TAC and stop it with this secondary trigger. The results are shown in Fig. 11. The signals marked in red are any signal that are produced by two overlapping events. This analysis also provides a way of measuring the effective pileups within an experiment, which, as we have found, are typically an order of magnitude less (10^3 pile-ups per second vs 10^4 pps) than the "good" signal events.

4. Experimental Results

In order to validate the operation of *Encore* as well as the analysis method employed, we performed a series of experiments with well-known systems and compared the data obtained with *Encore* to published data.

4.1. Fusion Reactions

Here, we discuss the fusion excitation functions of the stable systems ^{16}O + ^{12}C and ^{19}F + ^{12}C as measured with *Encore* at the John D. Fox laboratory at FSU. These measurements were part of an experimental campaign to understand the possible influence of the halo first excited state in ^{17}F on the fusion process [23].

A ^{16}O primary beam was used to produce a ^{17}F radioactive beam via the ^{16}O(d,n)^{17}F reaction. A liquid nitrogen-cooled gas cell was filled with deuterium gas and bombarded by a primary ^{16}O beam at 91.5 MeV. The radioactive ^{17}F beam at 61.5 MeV at a rate of 600 pps was delivered to *Encore* using the RESOLUT radioactive beam facility. However, part of the primary ^{16}O beam with the same rigidity as the ^{17}F reached *Encore* at 58.1 MeV and at a rate of 1100 pps. Measurements with ^{16}O and ^{17}F were performed simultaneously. The time-of-flight of the beams was used with strip 0 in *Encore* to separate the different beam components as it is shown in Fig. 4.

Encore was filled with CH_4 gas at 168 torr. Under these conditions, the fusion excitation function of the ^{16}O + ^{12}C system was measured in the energy range of E_{cm} = 8 MeV - 16 MeV. Results from this measurement are shown in Fig. 12 in comparison with existing published data [24–31]. The error bars in the cross sections are statistical while the error bars in the energy are due to the size of the strips in the segmented anode. The good agreement between our measurement with *Encore* and previous sets of data, especially the reproduction of the structures in the fusion excitation function, give us confidence in the analysis procedure used.

A separate experiment was performed to measure the fusion excitation function of the ^{19}F + ^{12}C system. A 65 MeV stable ^{19}F beam was delivered to *Encore* at a rate of 1000 pps. In this experiment, *Encore* was filled with 131 torr of CH_4 gas. The measured fusion excitation function of the ^{19}F + ^{12}C system is shown in Fig. 13 along with previous published data [24, 32, 33]. The error bars in the cross sections are statistical while the error bars in the energy are due to the size of the strips in the segmented anode. The agreement between our measurement and previous sets of data shows consistency of the analysis procedure.

4.2. (α,p) and (α,n) Reactions

The flexibility of the *Encore* detector allows it to be used with different counting gases. In particular, measurements with helium gas are of relevance in nuclear astrophysical scenarios.

We have successfully used *Encore* to measure ^{18}O(α,n)^{21}Ne and ^{18}O(α,p)^{21}F reactions simultaneously. For this experiment, *Encore* was filled with pure helium gas. A 52 MeV ^{18}O beam at a rate of 10,000

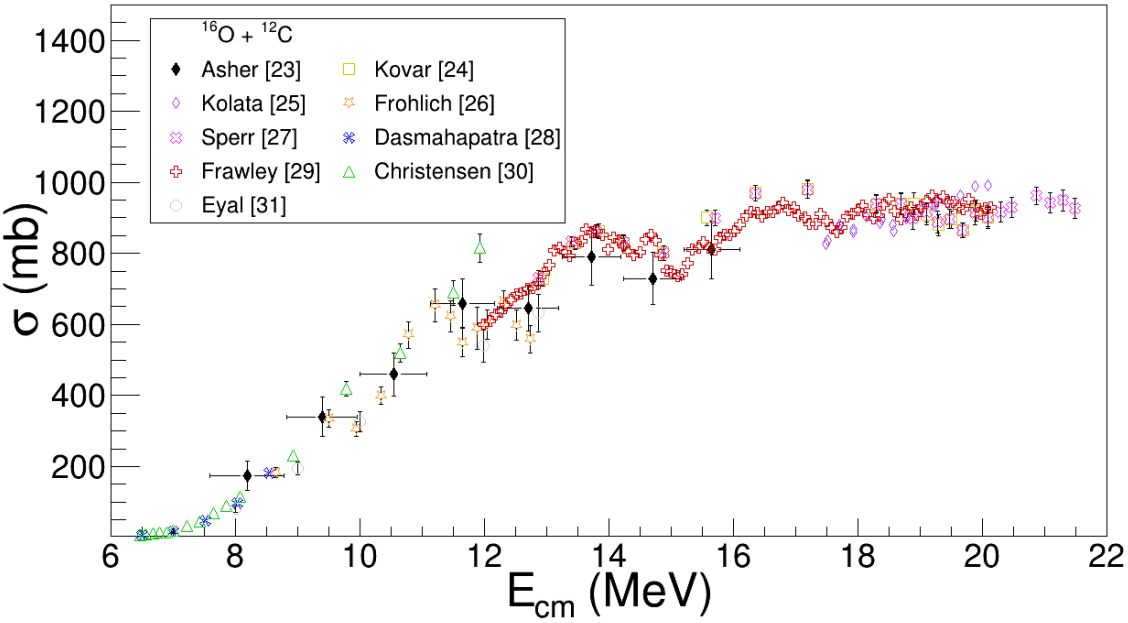

Figure 12: Results of the experimental fusion cross sections measured with *Encore* [23] for the ^{16}O + ^{12}C system compared with existing data from Refs. [24–31]. Good agreement is shown between the current measurement and previously published data.

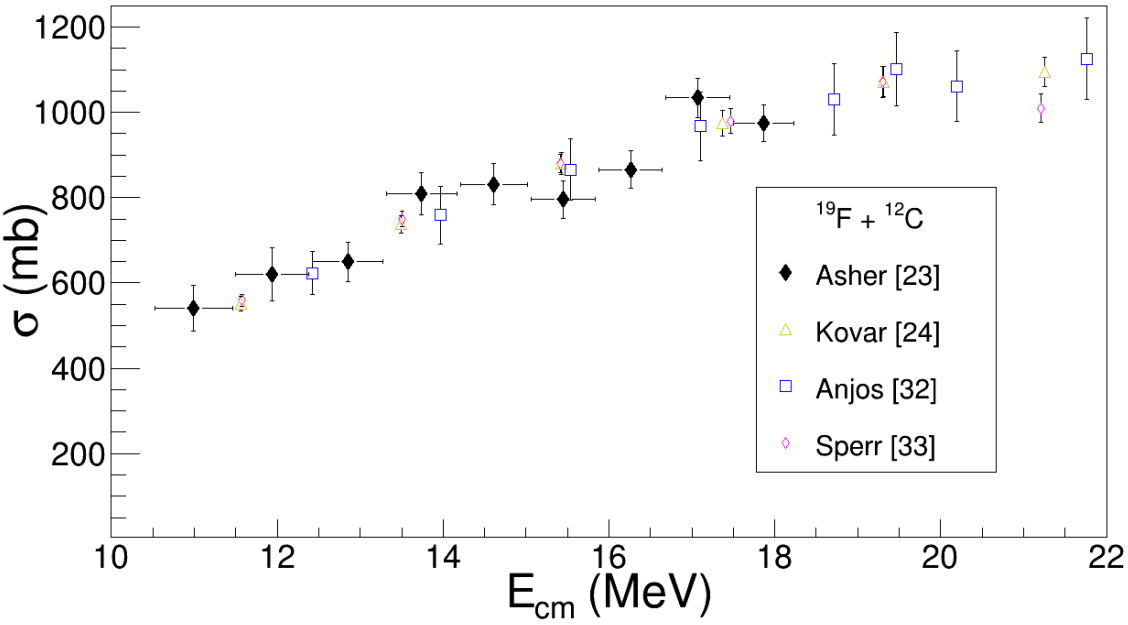

Figure 13: Results of the experimental fusion cross sections of the ^{19}F+ ^{12}C system measured with *Encore* [23] in comparison with existing data from Refs. [24, 32, 33]. Good agreement is observed between our measurement and data from literature.

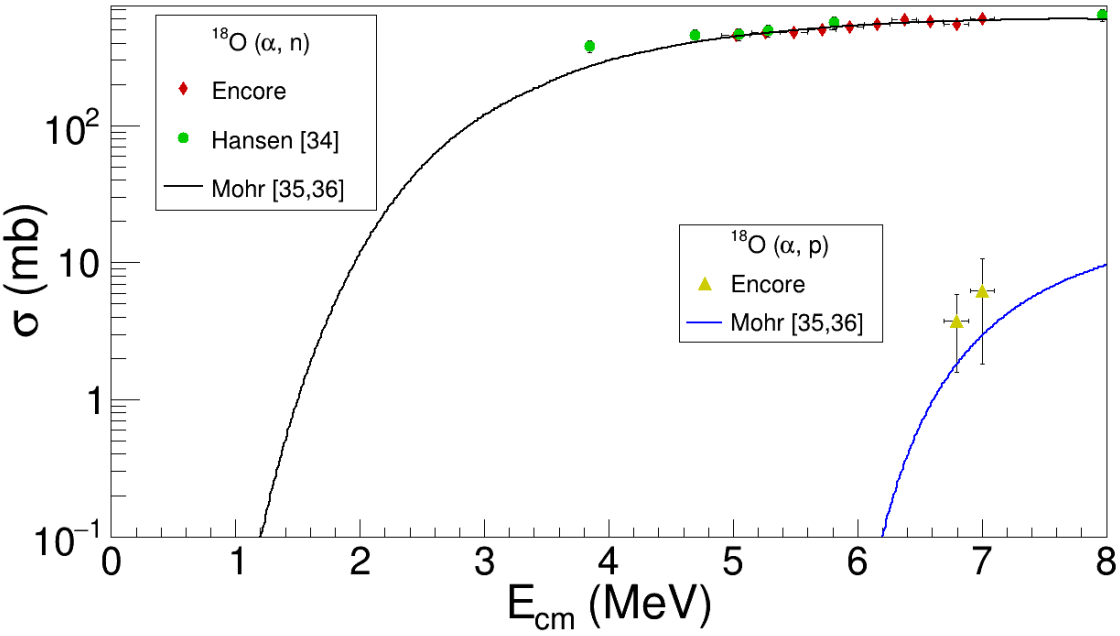

Figure 14: Results of the cross sections for the ^{18}O(α,n)^{21}Ne and ^{18}O(α,p)^{21}F reactions simultaneously measured with *Encore*. The measured cross sections are compared to statistical model calculations performed by P. Mohr [35, 36] and experimental data by Hansen et al. [34](energy error-bars in the data from ref. [34] are large and omitted for clarity). The y-axis for the ^{18}O(α,n) reaction is on the left side where cross sections are shown in linear scale. The y-axis for the ^{18}O(α,p) reaction is on the right side where the cross sections are shown in log scale. The ^{18}O(α,p) cross sections are about two orders of magnitude smaller than the ^{18}O(α,n) reactions in the measured energy range, thus the data points shown are upper limits on the cross section for the ^{18}O(α,p)^{21}F reaction.

pps was delivered to *Encore*, which was filled with 404 torr of helium gas. The energy and pressure in the detector are such that both channels, (α,p) and (α,n), are open in the first 8 strips. However, the (α,p) cross sections are only of the order of a few milibarns or less in this energy region as shown by statistical model calculations. Therefore, only upper limits for the (α,p) cross sections could be extracted for two of the early strips in the detector. Results of our measured cross sections are shown in Fig. 14. Very scarce experimental data are available for these systems. Our results are compared with data from ref. [34] and with statistical model calculations by P. Mohr [35, 36]. The measured (α,n) data agrees very well with the previous measurement and with the calculations. Despite the small cross sections for the (α,p) reaction, there is still very good agreement between our measurements and statistical model calculations that demonstrate the capabilities of *Encore*.

5. Summary and Outlook

In summary, *Encore* is an active target detector developed at FSU that measures energy losses as the beam travels through the detector using a segmented anode, thereby identifying reaction products and unreacted beam particles. *Encore* allows for the measurement of a large portion of the reaction excitation function using a single beam energy. Several gases can be used in the detector. We have measured the ^{16}O + ^{12}C and ^{19}F + ^{12}C fusion reactions using CH_4 gas. The ^{18}O(α,p)^{21}F and ^{18}O(α,n)^{21}Ne reactions were measured using helium gas in the detector. The results were compared with existing data and statistical model calculations, showing a good agreement among them.

Encore is a portable, versatile, highly-efficient, self-normalizing, active target detector optimized for use with low intensity radioactive beams. In the future, other gases (Ne, Ar, Kr) can be used to explore different mass ranges and Z dependencies on the measured reactions and to study other reaction processes like fission. Further improvements include the use of digital electronics as well as residue identification.

Acknowledgements

This work was supported by the National Science Foundation under grants PHY-1712953 and PHY-2012522, and by the State of Florida. The authors would like to thank E. Rehm, M. Avila and D. Santiago-Gonzalez for their helpful discussions and P. Mohr for providing the calculations of the cross sections for the ^{18}O(α,p) and ^{18}O(α,n) reactions.

6. References

References

[1] P. Carnelli, S. Almaraz-Calderon, K. Rehm, M. Albers, M. Alcorta, P. Bertone, B. Digiovine, H. Esbensen, J. F. Niello, D. Henderson, C. Jiang, J. Lai, S. Marley, O. Nusair, T. Palchan-Hazan, R. Pardo, M. Paul, C. Ugalde, Multi-sampling ionization chamber (music) for measurements of fusion reactions with radioactive beams, Nuclear Instruments and Methods in Physics Research Section A: Accelerators, Spectrometers, Detectors and Associated Equipment 799 (2015) 197 – 202. doi:https://doi.org/10.1016/j.nima.2015.07.030.
URL http://www.sciencedirect.com/science/article/pii/S0168900215008591

[2] C. Demonchy, W. Mittig, H. Savajols, P. Roussel-Chomaz, M. Chartier, B. Jurado, L. Giot, D. Cortina-Gil, M. Caamano, G. Ter-Arkopian, A. Fomichev, A. Rodin, M. Golovkov, S. Stepantsov, A. Gillibert, E. Pollacco, A. Obertelli, H. Wang, Maya, a gaseous active target, Nuclear Instruments and Methods in Physics Research Section A: Accelerators, Spectrometers, Detectors and Associated Equipment 573 (1) (2007) 145–148, proceedings of the 7th International Conference on Position-Sensitive Detectors. doi:https://doi.org/10.1016/j.nima.2006.11.025.
URL https://www.sciencedirect.com/science/article/pii/S0168900206022558

[3] E. Koshchiy, J. Blackmon, G. Rogachev, I. Wiedenhöver, L. Baby, P. Barber, D. Bardayan, J. Belarge, D. Caussyn, E. Johnson, K. Kemper, A. Kuchera, L. Linhardt, K. Macon, M. MatoÅ¡, B. Rasco, D. Santiago-Gonzalez, Anasen: The array for nuclear astrophysics and structure with exotic nuclei, Nuclear Instruments and Methods in Physics Research Section A: Accelerators, Spectrometers, Detectors and Associated Equipment 870 (2017) 1–11. doi:https://doi.org/10.1016/j.nima.2017.07.030.
URL https://www.sciencedirect.com/science/article/pii/S0168900217307726

[4] A. Laird, P. Amaudruz, L. Buchmann, S. Fox, B. Fulton, D. Gigliotti, T. Kirchner, P. Mumby-Croft, R. Openshaw, M. Pavan, J. Pearson, G. Ruprecht, G. Sheffer, P. Walden, Status of tactic: A detector for nuclear astrophysics, Nuclear Instruments and Methods in Physics Research Section A: Accelerators, Spectrometers, Detectors and Associated Equipment 573 (1) (2007) 306–309, proceedings of the 7th International Conference on Position-Sensitive Detectors. doi:https://doi.org/10.1016/j.nima.2006.10.384.
URL https://www.sciencedirect.com/science/article/pii/S0168900206021553

[5] E. Koshchiy, G. Rogachev, E. Pollacco, S. Ahn, E. Uberseder, J. Hooker, J. Bishop, E. Aboud, M. Barbui, V. Goldberg, C. Hunt, H. Jayatissa, C. Magana, R. O. Dwyer, B. Roeder, A. Saastamoinen, S. Upadhyayula, Texas active target (texat) detector for experiments with rare isotope beams, Nuclear Instruments and Methods in Physics Research Section A: Accelerators, Spectrometers, Detectors and Associated Equipment 957 (2020) 163398. doi:https://doi.org/10.1016/j.nima.2020.163398.
URL https://www.sciencedirect.com/science/article/pii/S0168900220300073

[6] D. Suzuki, M. Ford, D. Bazin, W. Mittig, W. Lynch, T. Ahn, S. Aune, E. Galyaev, A. Fritsch, J. Gilbert, F. Montes, A. Shore, J. Yurkon, J. Kolata, J. Browne, A. Howard, A. Roberts, X. Tang, Prototype at-tpc: Toward a new generation active target time projection chamber for radioactive beam experiments, Nuclear Instruments and Methods in Physics Research Section A: Accelerators, Spectrometers, Detectors and Associated Equipment 691 (2012) 39–54. doi:https://doi.org/10.1016/j.nima.2012.06.050.
URL https://www.sciencedirect.com/science/article/pii/S0168900212007164

[7] Y. Mizoi, T. Fukuda, Y. Matsuyama, T. Miyachi, J. Nakano, N. Fukuda, M. Hirai, H. Kobinata, Y. Watanabe, H. Sakurai, Y. Watanabe, A. Yoshida, Multiple-sampling and tracking proportional chamber for nuclear reactions with low-energy radioactive isotope beams, Nuclear Instruments and Methods in Physics Research Section A: Accelerators, Spectrometers, Detectors and Associated Equipment 431 (1) (1999) 112–122. doi:https://doi.org/10.1016/S0168-9002(99)00253-3.
URL https://www.sciencedirect.com/science/article/pii/S0168900299002533

[8] M. Cwiok, W. Dominik, Z. Janas, A. Korgul, K. Miernik, M. Pfutzner, M. Sawicka, A. Wasilewski, Optical time projection chamber for imaging of two-proton decay of ^{45}fe nucleus, IEEE Transactions on Nuclear Science 52 (6) (2005) 2895–2899. doi:10.1109/TNS.2005.862796.

[9] W. Christie, J. Romero, F. Brady, C. Tull, C. Castaneda, E. Barasch, M. Webb, J. Drummond, H. Crawford, I. Flores, D. Greiner, P. Lindstrom, H. Sann, J. Young, A multiple sampling ionization chamber (music) for measuring the charge of relativistic heavy ions, Nuclear Instruments and Methods in Physics Research Section A: Accelerators, Spectrometers, Detectors and Associated Equipment 255 (3) (1987) 466–476. doi:https://doi.org/10.1016/0168-9002(87)91213-7.
URL https://www.sciencedirect.com/science/article/pii/0168900287912137

[10] P. F. F. Carnelli, S. Almaraz-Calderon, K. E. Rehm, M. Albers, M. Alcorta, P. F. Bertone, B. Digiovine, H. Esbensen, J. O. F. Niello, D. Henderson, C. L. Jiang, J. Lai, S. T. Marley, O. Nusair, T. Palchan-Hazan, R. C. Pardo, M. Paul, C. Ugalde, Measurements of fusion reactions of low-intensity radioactive carbon beams on ^{12}C and their implications for the understanding of x-ray bursts, Phys. Rev. Lett. 112 (2014) 192701. doi:10.1103/PhysRevLett.112.192701.
URL https://link.aps.org/doi/10.1103/PhysRevLett.112.192701

[11] M. Avila, K. Rehm, S. Almaraz-Calderon, A. Ayangeakaa, C. Dickerson, C. Hoffman, C. Jiang, B. Kay, J. Lai, O. Nusair, R. Pardo, D. Santiago-Gonzalez, R. Talwar, C. Ugalde, Study of (α,p) and (α,n) reactions with a multi-sampling ionization chamber, Nuclear Instruments and Methods in Physics Research Section A: Accelerators, Spectrometers, Detectors and Associated Equipment 859 (2017) 63 – 68. doi:https://doi.org/10.1016/j.nima.2017.03.060.
URL http://www.sciencedirect.com/science/article/pii/S0168900217304187

[12] R. Talwar, M. J. Bojazi, P. Mohr, K. Auranen, M. L. Avila, A. D. Ayangeakaa, J. Harker, C. R. Hoffman, C. L. Jiang, S. A. Kuvin, B. S. Meyer, K. E. Rehm, D. Santiago-Gonzalez, J. Sethi, C. Ugalde, J. R. Winkelbauer, Experimental study of ^{38}Ar + α reaction cross sections relevant to the ^{41}Ca abundance in the solar system, Phys. Rev. C 97 (2018) 055801. doi:10.1103/PhysRevC.97.055801.
URL https://link.aps.org/doi/10.1103/PhysRevC.97.055801

[13] B. B. Back, J. A. Clark, R. C. Pardo, K. E. Rehm, G. Savard, Astrophysics experiments with radioactive beams at atlas, AIP Advances 4 (4) (2014) 041005. arXiv:https://doi.org/10.1063/1.4865588, doi:10.1063/1.4865588.
URL https://doi.org/10.1063/1.4865588

[14] P. Carnelli, Measurement of fusion cross sections of carbon isotopes using an active target, Ph.D. thesis, National University of General San Martin (2014).

[15] T. E. Bortner, G. S. Hurst, W. G. Stone, Drift velocities of electrons in some commonly used counting gases, Review of Scientific Instruments 28 (2) (1957) 103–108. arXiv:https://doi.org/10.1063/1.1715825, doi:10.1063/1.1715825.
URL https://doi.org/10.1063/1.1715825

[16] W. Blum, L. Rolandi, Particle Detection with Drift Chambers, Springer-Verlag, 1964.

[17] MKS, Mks capacitance manometers, https://www.mksinst.com/f/627f-heated-capacitance-manometers, ac-

cessed: 2021-03-01.
[18] I. Wiedenhöver, L. T. Baby, D. Santiago-Gonzalez, A. Rojas, J. C. Blackmon, G. V. Rogachev, J. Belarge, E. Koshchiy, A. N. Kuchera, L. E. Linhardt, J. Lail, K. T. Macon, M. Matos, B. C. Rascol, Studies of Exotic Nuclei at the Resolut Facility of Florida State University, in: Fission and Properties of Neutron-Rich Nuclei - Proceedings of the Fifth International Conference on ICFN5. Edited by Hamilton Joseph H & Ramayya Akunuri V. Published by World Scientific Publishing Co. Pte. Ltd, 2014, pp. 144–151. doi:10.1142/9789814525435_0015.
[19] D. Santiago-Gonzalez, private communication.
[20] O. B. Tarasov, D. Bazin, LISE++: Radioactive beam production with in-flight separators, Nuclear Instruments and Methods in Physics Research B 266 (19-20) (2008) 4657–4664. doi:10.1016/j.nimb.2008.05.110.
[21] J. F. Ziegler, M. Ziegler, J. Biersack, Srim - the stopping and range of ions in matter (2010), Nuclear Instruments and Methods in Physics Research Section B: Beam Interactions with Materials and Atoms 268 (11) (2010) 1818–1823, 19th International Conference on Ion Beam Analysis. doi:https://doi.org/10.1016/j.nimb.2010.02.091.
URL https://www.sciencedirect.com/science/article/pii/S0168583X10001862
[22] H. Paul, D. Sánchez-Parcerisa, A critical overview of recent stopping power programs for positive ions in solid elements, Nuclear Instruments and Methods in Physics Research Section B: Beam Interactions with Materials and Atoms 312 (2013) 110–117. doi:https://doi.org/10.1016/j.nimb.2013.07.012.
URL https://www.sciencedirect.com/science/article/pii/S0168583X13007520
[23] B. W. Asher, S. Almaraz-Calderon, V. Tripathi, K. W. Kemper, L. T. Baby, N. Gerken, E. Lopez-Saavedra, A. B. Morelock, J. F. Perello, I. Wiedenhöver, N. Keeley, Experimental study of the ^{17}F +^{12} C fusion reaction and its implications for fusion of proton-halo systems, Phys. Rev. C 103 (2021) 044615. doi:10.1103/PhysRevC.103.044615.
URL https://link.aps.org/doi/10.1103/PhysRevC.103.044615
[24] D. G. Kovar, D. F. Geesaman, T. H. Braid, Y. Eisen, W. Henning, T. R. Ophel, M. Paul, K. E. Rehm, S. J. Sanders, P. Sperr, J. P. Schiffer, S. L. Tabor, S. Vigdor, B. Zeidman, F. W. Prosser, Systematics of carbon- and oxygen-induced fusion on nuclei with $12 \leq a \leq 19$, Phys. Rev. C 20 (1979) 1305–1331. doi:10.1103/PhysRevC.20.1305.
URL https://link.aps.org/doi/10.1103/PhysRevC.20.1305
[25] J. Kolata, R. Freeman, F. Haas, B. Heusch, A. Gallmann, On the fusion cross section for ^{16}O + ^{12}C, Phys. Lett. B 65 (4) (1976) 333 – 336. doi:https://doi.org/10.1016/0370-2693(76)90235-5.
URL http://www.sciencedirect.com/science/article/pii/0370269376902355
[26] H. Fröhlich, P. Dück, W. Galster, W. Treu, H. Voit, H. Witt, W. Kühn, S. Lee, Oscillations in the excitation function for complete fusion of ^{16}O+^{12}C at low energies, Phys. Lett. B 64 (4) (1976) 408 – 410. doi:https://doi.org/10.1016/0370-2693(76)90107-6.
URL http://www.sciencedirect.com/science/article/pii/0370269376901076
[27] P. Sperr, S. Vigdor, Y. Eisen, W. Henning, D. G. Kovar, T. R. Ophel, B. Zeidman, Oscillations in the excitation function for complete fusion of ^{16}O+^{12}C, Phys. Rev. Lett. 36 (1976) 405–408. doi:10.1103/PhysRevLett.36.405.
URL https://link.aps.org/doi/10.1103/PhysRevLett.36.405
[28] B. Dasmahapatra, B. Čujec, F. Lahlou, Fusion cross sections for ^{16}O + ^{13}C at low energies, Nuclear Physics A 394 (1) (1983) 301 – 311. doi:https://doi.org/10.1016/0375-9474(83)90175-6.
URL http://www.sciencedirect.com/science/article/pii/0375947483901756
[29] A. D. Frawley, N. R. Fletcher, L. C. Dennis, Resonances in the ^{16}O + ^{12}C fusion cross section between $E_{\mathrm{c.m.}}$ = 12and20 mev, Phys. Rev. C 25 (1982) 860–865. doi:10.1103/PhysRevC.25.860.
URL https://link.aps.org/doi/10.1103/PhysRevC.25.860
[30] P. Christensen, Z. Switkowskiw, R. Dayras, Sub-barrier fusion measurements for ^{12}C+^{16}O, Nuclear Physics A 280 (1) (1977) 189 – 204. doi:https://doi.org/10.1016/0375-9474(77)90303-7.
URL http://www.sciencedirect.com/science/article/pii/0375947477903037
[31] Y. Eyal, M. Beckerman, R. Chechik, Z. Fraenkel, H. Stocker, Nuclear size and boundary effects on the fusion barrier of oxygen with carbon, Phys. Rev. C 13 (1976) 1527–1535. doi:10.1103/PhysRevC.13.1527.
URL https://link.aps.org/doi/10.1103/PhysRevC.13.1527
[32] R. M. Anjos, V. Guimares, N. Added, N. Carlin Filho, M. M. Coimbra, L. Fante, M. C. S. Figueira, E. M. Szanto, C. F. Tenreiro, A. Szanto de Toledo, Effect of the entrance channel mass asymmetry on the limitation of light heavy-ion fusion cross sections, Phys. Rev. C 42 (1990) 354–362. doi:10.1103/PhysRevC.42.354.
URL https://link.aps.org/doi/10.1103/PhysRevC.42.354
[33] P. Sperr, T. H. Braid, Y. Eisen, D. G. Kovar, F. W. Prosser, J. P. Schiffer, S. L. Tabor, S. Vigdor, Fusion cross sections of light heavy-ion systems: Resonances and shell effects, Phys. Rev. Lett. 37 (1976) 321–323. doi:10.1103/PhysRevLett.37.321.
URL https://link.aps.org/doi/10.1103/PhysRevLett.37.321
[34] L. F. Hansen, J. D. Anderson, J. W. McClure, B. A. Pohl, M. L. Stelts, J. J. Wesolowski, C. Wong, The (α, n) cross sections

on ^{17}o and ^{18}o between 5 and 12.5 mev, Nuclear Physics A 98 (1) (1967) 25–32. doi:https://doi.org/10.1016/0375-9474(67)90895-0.
URL https://www.sciencedirect.com/science/article/pii/0375947467908950
[35] P. Mohr, Uncertainty of the astrophysical ^{17,18}O$(\alpha,n)^{20,21}$Ne reaction rates and the applicability of the statistical model for nuclei with $a \lesssim 20$, Phys. Rev. C 96 (2017) 045808. doi:10.1103/PhysRevC.96.045808.
URL https://link.aps.org/doi/10.1103/PhysRevC.96.045808
[36] P. Mohr, private communication.